Bi-Metallic films of Gold, MXene, and Graphene nano film-based Surface Plasmon Resonance Sensor for Malaria Detection: A Numerical Analysis

Arun Uniyal
DIT University
Brajlata Chauhan
DIT University
Amrindra Pal (amrindra.ieee@gmail.com)
DIT University

Research Article

Keywords: Kretschmann structure, Reflectance, Surface plasmon resonance, MXene, Graphene, Malaria detection

Posted Date: June 24th, 2022

DOI: https://doi.org/10.21203/rs.3.rs-1766754/v1

Bi-Metallic films of Gold, MXene, and Graphene nano film-based Surface Plasmon Resonance Sensor for Malaria Detection: A Numerical Analysis

Arun Uniyal*[a], Brajlata Chauhan *Amrindra Pal[a]
[a] Department of ECE, DIT University, Dehradun-248009, India
*Corresponding Author: Email address: arunavenue@gmail.com

Abstract: In this proposed work, an SPR-based biosensor with dual nanofilms of a gold metal, 2-Dimensional MXene, and graphene has been proposed to detect different malaria stages. The principal obeyed by the sensor design is attenuated total reflection (ATR) with a modified Kretschmann-based configuration. Numerical computational results give the higher sensitivity for our proposed design as 227.9 degree/RIU (for single MXene and dual graphene layers at RI variation of 1.33 to 1.38 with a change of 0.01) and 258.28 degree/RIU(for trophozoite stage of malaria disease), with other performance parameters like DA computed as equal to 0.14 degree^{-1} , QF as 31 RIU^{-1} and 35.5 RIU^{-1}, FWHM as 7.35 degree and 7.27 degree for single MXene, dual graphene nanofilms and trophozoite stage respectively. The suggested biosensor can diagnose the various stages of severe malaria disease by measuring the refractive index alteration in red blood cells (RBCs).

Keywords: Kretschmann structure, Reflectance, Surface plasmon resonance, MXene, Graphene, Malaria detection

Introduction:

Surface plasmon resonance (SPR) based biosensors are gaining popularity in detecting analytes, chemicals, biomolecules, bacteria, and viruses. The discovery of the SPR has improved the chemical sensor and biosensor [1][2]. Fiber optic and prism-based SPR sensors are available for different sensing applications [1]. Surface plasmons (SPs) are oscillating electromagnetic waves that propagate above a metal surface and are produced with a combination of free vibrating electrons and photons. The SPs are excited when the sensing medium's refractive index (R.I.) changes. The R.I. variation of the sensing medium causes a change in the resonance angle position and results in the change in the position of the dip on the resonance [1]. The two basic configurations used in prism coupled based SPR sensors are Otto [2] and Kretschmann [3]. A metal must have electrons in the conduction band (follows the free electron model) that can resonate with light at an appropriate wavelength to be helpful for the SPR mechanism [6]. The principal followed by this configuration is attenuated total reflection (ATR) [4]. In the prism-based configuration, a TM, p-polarized light strikes the one

interface of the prism it penetrates through thin metal film, giving an evanescent wave. Ultimately generates the SP at the boundary (between metal-analyte). In Otto configuration, an air gap is provided between prism and metal, but in Kretschmann configuration, one prism face is attached with metal. The easy practical implementation and efficient generation of plasmons in Kretschmann configuration make it a suitable choice for SPR sensing applications [5][6][7]. The SPR sensing technique has proven to be more advantageous for real-time applications in cancer cell detection, DNA hybridization, antibody characterization, protein conformation, and detection of bacteria such as Pseudomonas and various viruses like Covid-19, SARS, etc.[8]. Based on SPR technology, some popular applications like gas sensing, foodborne marker screening, environmental monitoring, disease diagnosis, and food safety have been developed during the last three decades [9][10][11].

Plasmonic metals such as silver, gold, aluminum, copper and nickel, cobalt, etc., can be used in the SPR sensor [12][13][14][15][16]. The free-electron criterion model criterion is satisfied by these metallic elements. The inclusion of Au in this study is due to the upper hand (more merits) over Ag. The properties like its greater corrosion resistance, higher stability, and sensitivity [17]. On the other hand, Ag easily oxidizes and shows less sensitivity. The other metals like Al and Cu easily oxidize, and additional layers for the protection are needed, making the design complex [18]. Since with less adsorbing properties of a metal film, 2 D materials are introduced above the metal layers mounted over the glass prism to improve the biosensor's performance and work as a protecting layer for the metal. With advancements in the technology sector, sensing applications use 2D materials [19]. The most commonly used 2 D materials like graphene[20], black phosphorus (BP) [21], Molybdenum disulfide (MoS_2) [22], perovskite materials [23], Bi_2Te_3 [24], sulfosalt[6], etc. shows rapid popularity in SPR based biosensors due to their optoelectrical properties. This study employs the basic recognition element (BRE) over the metal (Au_1) film. The properties of graphene-like greater robustness and mobility, single-atom thickness, highly flexible and durable, unrivaled opto-thermal, and at room temperature notable conductivity, zero-gap, less noise, etc., made a strong choice as BRE in the biosensors [25][26]. Although these features of 2D material are very inspiring when used in the optical research field, somehow, its thickness control is to be taken extra care compared to bulk materials during large-scale fabrication. So, to control the thickness of 2 D materials, several methods have been introduced such as Chemical Vapor Deposition (CVD), mechanical exfoliation, metal-organic CVD, and atomic layer deposition (ALD) [18]. Wu et al. [27] proposed an SPR biosensor design with graphene as a core material

with an Al metal layer and dual films of MoS_2. It gives a higher performance in terms of sensitivity as high as 190.83 degree/RIU. Mostufa et al. [28] proposed an SPR mechanism-based biosensor (Au+$PtSe_2$+Graphene) for the hemoglobin detection in blood and glucose in urine and attained 200 degree/RIU sensitivity. Dong et al. [29] demonstrated a SPR biosensor using Ag/PbS/ graphene heterogeneous design and numerically computed five times greater sensitivity than the traditional design. Recently, Moznuzzaman et.al [30] presented a theoretical study of virus (SARS-COV-2) applying TiO_2/Ag/$MoSe_2$/Graphene films over prism and achieved 194 degree/RIU (sensitivity), QF as 54.04 1/RIU and DA as 0.2702. Guo et al. [31] numerically simulated a SPR biosensor with (TiO_2 + ZnO + Au + MoS_2 + Graphene oxide) modified Kretschmann configuration and 210.75 degree/RIU sensitivity has been achieved. Research work by Xu et al. proposed a Kretschmann based SPR biosensor using Au_1/TMDC/Au_2/$Ti_3C_2T_x$ and achieved the sensitivity of 198 degree/RIU[1].

MXene is a new emerging 2D material recently gaining popularity among the researchers due to its electrical properties like high conductivity, alongside the mechanical properties like it can access hydrophilic surfaces easily[32], greater spacing between interlayers, higher thermal stability and surface area [33][34][35]. It has a tightly packed hexagonal crystal structure with optical properties like bandgap adjustment and higher light and matter interactions. Its general formula is $M_{n+1}X_nT_x$, here M, X, n and T_x represents transition metal, C or/and N, an integer between 1 and 3, and surface functional groups [33]. Earlier research works using MXene in sensing-based applications like gas sensors, electrochemical sensors, etc. Other than these other applications like energy storage, purifying water, photo, chemical catalysts, etc.

Malaria is a disease that mainly spreads due to a parasite infecting a female mosquito. It can cause severe health hazards, sometimes to death also. A recent report by WHO gives the data that in the year 2018, across the world, 228 million cases of malaria were reported [36]. The diagnosis of malaria should be done in the early stages; otherwise, it is difficult to cure [37]. The optical characteristics of red blood cells (RBCs) in the human blood play an important role in determining the phases of malaria illnesses. Normal, Ring, Trophozoite, and Schizont are the different stages of malaria disease. The prime constituents of RBC are water and hemoglobin, as the concentration in hemoglobin makes the R.I. variation of RBC. In Table 1, these stages of malaria disease with RI of RBC have been summarized:

Table 1: Stages of malaria with average R.I. of RBC

Malaria stage	Average R.I. (RBC)	References
Normal (I)	1.402	[38][39]
Ring (II)	1.395	
Trophozoite (III)	1.381	
Schizont (IV)	1.371	

Section 2 gives the design methodology with the numerical analysis of the proposed SPR sensor. Section 3 consists of results and discussions of the proposed work. In the end, Section 4 concludes the proposed work.

2. Design consideration and theoretical model:

The proposed SPR sensor consists of five layers, namely metals (Au1 and Au2) nanofilms, 2D materials (MXene and graphene) structure, and a sensing layer. Figure 1(a) shows the proposed SPR. The multilayer structure of our proposed SPR sensor is shown with the help of Figure 1(b). Figure 1(b) shows how incident light is transmitted and reflected through the multilayered structure.

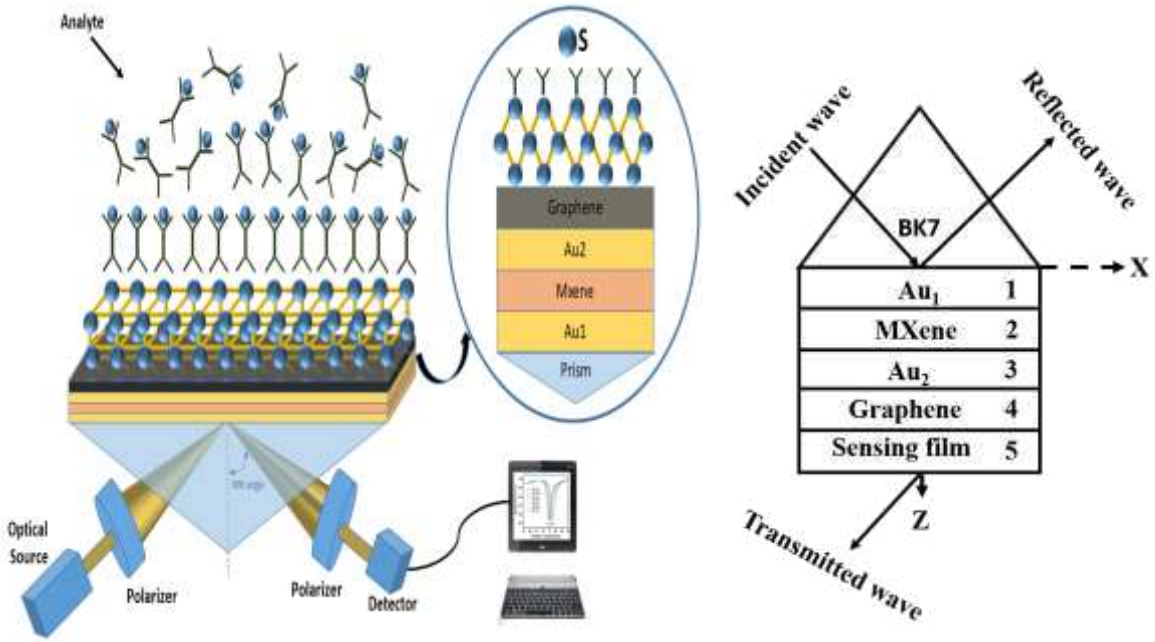

Figure 1. (a) Schematic of proposed SPR sensor (b) Layer structure of SPR sensor

2.1 Refractive index of Prism and other films:

The transverse magnetic, p-polarized light is incident on the one surface of the prism and reflected and comes out of the other surface. Here He-Ne laser source is used. A low refractive index prism is frequently used to stimulate surface plasmons because it boosts its excitation energy. This is because incident light's wave vector balances the surface plasmon's wave vector. A BK7 prism is a borosilicate crown glass prism. It is lead-free and arsenic-free and is widely used in optical biosensing applications. The transmission rate is between 350 nm and 2000 nm. Furthermore, because of its low refractive index than other glass prisms, it gives greater sensitivity. The BK7 prism demonstrates the most significant SPR viewpoint while retaining a respectable minimum reflectance [40]. The design parameters used in our proposed structure have been summarized in Table 2.

Table 2. SPR biosensor configuration parameters

Films	**Materials (BK7 Prism as base)**	**Width (nm)**	**R.I. at 633 nm**
1	Au (1st layer)	$D_1 = 45$	$0.18344 + \mathrm{i} * 3.4332$
2	MXene (2nd layer)	$D_2 = G * 0.993$	$2.38 + i * 1.33$
3	Au (3rd layer)	$D_3 = 3$	$0.18344 + \mathrm{i} * 3.4332$
4	Graphene (4th layer)	$D_4 = T * 2$	$3 + \mathrm{i} * 1.1491$
5	Sensing film (5th layer)	-	1.33+Δ n

For the BK7 prism, its R.I.is given by the Sellmeier equation [41]:

$$n_p = \left(\frac{\alpha_a \lambda^2}{\lambda^2 - \beta_a} + \frac{\alpha_b \lambda^2}{\lambda^2 - \beta_b} + \frac{\alpha_c \lambda^2}{\lambda^2 - \beta_c} + 1\right)^{1/2} \quad (1)$$

here, λ is the wavelength of the incident optical signal. The values for the constants given in equation 1 have been summarized in Table 2.

Table 2. Constants values in equation (1)

Constant	**Values**	**Constant**	**Values**
α_a	1.03961212	β_a	0.00600069867
α_b	0.231792344	β_b	0.0200179144
α_c	1.0104694	β_c	103.560653

For Au (metal), R.I. can be expressed by Drude Lorentz's model [42]:

$$n_{Au} = \left(1 - \frac{\lambda^2 * \lambda_c}{\lambda_p^2(\lambda_c + \lambda * i)}\right)^{1/2} \quad (2)$$

here, the value of λ_c (collision wavelength) is $8.9342 * 10^{-6}$ m and λ_p (plasma wavelength) is $1.6826 * 10^{-7}$ m.

2.2 Transfer matrix method (TMM):

A popular method used for reflectance computation; the transfer matrix method [43]. Using the N-layer matrix method, a theoretical study was conducted. Therefore, the characteristic matrix can be used to express the N-layer structure, as shown in equation 3.

$$T = \prod_K^{N-1} T_K = \begin{bmatrix} T_{11} & T_{12} \\ T_{21} & T_{22} \end{bmatrix} \quad (3)$$

$$\text{as } T_K = \begin{bmatrix} \cos\beta_k & -i(\sin\beta_k)/q_k \\ -iq_k\sin\beta_k & \cos\beta_k \end{bmatrix} \quad (4)$$

here, T_K is the k^{th} layer matrix, β_k is the optical admittance and q_k is the phase factor.

$$\beta_k = \frac{2\pi}{\lambda} d_k \sqrt[2]{\epsilon_k - n_1^2 \sin^2\theta_1}$$

$$q_k = \sqrt[2]{\epsilon_k - n_1^2 \sin^2\theta_1} \Big/ \epsilon_k$$

Here, θ_1 is the incidence angle at the BK7 prism,λ is the operating wavelength and ϵ_k is the dielectric constant and d_k is kth layer's thickness.

The coefficients of reflection of p-polarized (TM mode) incident wave are expressed as:

$$R_p = |r_p|^2 = \left(\frac{(T_{11} + T_{12}q_N)q_1 - (T_{21} + T_{22}q_N)}{(T_{11} + T_{12}q_N)q_1 + (T_{21} + T_{22}q_N)}\right) \quad (5)$$

2.3 Parameters for SPR sensor performance:

The parameters which define the SPR sensor's performance, such as sensitivity(S), minimum reflectance (R_m), full width half maximum (FWHM), the figure of merit (FOM), and detection accuracy (DA), have been computed. For the best performance of the SPR sensor, the S, DA, and FOM should be high [44], and the value of FWHM should be low.

2.3.1 Sensitivity (S):

The sensitivity (S) is defined as the ratio of the deviation in the resonance angle of incidence to the change in the sensing medium's refractive index. The sensitivity can be expressed by the formula:

$$S = \frac{\Delta\theta_{res}}{\Delta n} \text{ (in degree/RIU)} \quad (6)$$

here, $\Delta\theta_{res}$= change in the resonance angle, Δn= change in refractive index of the sensing film

2.3.2 Full width half maxima (FWHM):

The full width quantitatively describes the width and sharpness of the reflectance curve at half maximum (FWHM). The FWHM can be expressed by the formula:

$$\text{FWHM} = \theta_2 - \theta_1 \text{(in degree)} \quad (7)$$

2.3.3 Figure of merit (FOM) or Quality factor (QF):

This parameter describes the resolution of the sensor. It is the ratio of the sensitivity and the FWHM. It is generally expressed with the relation:

$$QF = S/FWHM \text{ (in } RIU^{-1}) \quad (8)$$

2.3.4 Detection accuracy (DA) or signal to noise ratio (SNR):

It is the reciprocal of FWHM. Its determination is done with the help of the SPR curve.

It is defined by:

$$\text{DA or SNR} = 1/FWHM \text{ (in degree}^{-1}) \quad (9)$$

2.4 Field distribution computation:

The electric field distribution of the TM (p-polarized) light within each layer displays the evanescent field augmentation of the proposed structure under various conditions. The generation of the evanescent field above the analysis interface is critical for the surface resonance phenomena since the sensing process is done on the analyte's boundary. Therefore, using the reflectance and transmittance of the TM polarized light, compute the E and H field distribution within the first layer using the total characteristics matrix equation presented below [45]:

$$\begin{bmatrix} H_{y1}(z) \\ -E_{x1}(z) \end{bmatrix} = P_1(z).\begin{bmatrix} 1+r_p \\ q_1(1-r_p) \end{bmatrix} H_y^{inc}, z_1 \le z \le z_2 \quad (10)$$

Here $H_{y1}(z)$ and $E_{x1}(z)$ are magnetic and electric fields, H_y^{inc} = incident magnetic field amplitude and r_p = reflection coefficient.

$$\text{here, } P_1(z) = \begin{bmatrix} \cos(\beta_{k(at\ z)}) & i/q_1 \sin(\beta_{k(at\ z)}) \\ iq_1 \sin(\beta_{k(at\ z)}) & \cos(\beta_{k(at\ z)}) \end{bmatrix} \quad (11)$$

In the same manner, these field distributions within the layer $j \ge 2$ are given by:

$$\begin{bmatrix} H_{yj}(z) \\ -E_{xj}(z) \end{bmatrix} = P_j(z) * \prod_{j-1}^{1} P(z = z_i + d_i) * \begin{bmatrix} 1+r_p \\ q_j(1-r_p) \end{bmatrix} H_y^{inc}, z_j \le z \le z_{j+1} \quad (12)$$

$$\text{here, Propagation matrix, } P_j(z) = \begin{bmatrix} \cos(\beta_{k(at\ z=z-1)}) & i/q_j \sin(\beta_{k(at\ z=z-1)}) \\ iq_j \sin(\beta_{k(at\ z=z-1)}) & \cos(\beta_{k(at\ z=z-1)}) \end{bmatrix} \quad (13)$$

2.5 Experiment possibilities

The fabrication steps of different layers for our proposed sensor have been done, giving the final design for the SPR chip. The coupling glass prism was initially dipped in the solution (acetone vapor + methanol + deionized water), earlier coupled to the gold nanolayer. Over the prism glass, the physical vapor deposition (PVD) of both gold layers is done by a thermal evaporator system [46]. The fabrication of the graphene nanolayer was performed using the Chemical vapor deposition (CVD) process [47]; afterward, this graphene layer chemically shifted to the MXene layer. The process of liquid exfoliation may be adopted for preparing the MXene layer [48]. The last step to be performed after the fabrication is the transfer of these layers of chips over the coupling prism, and the results are calculated with the help of a sensor setup. Generally, for sensing-based applications, deionized water has been inserted with the help of input flow cells in the sensing medium, and it contains impurities such as bacteria, viruses, etc. Then, this organic aqueous solution is poured above the sensor chip area for sensing purposes. Over a rotating table, the entire combination has been placed, and the resonance angle is set, as shown in figure 1. The output side of the coupling prism used has an optical detector that detects the light reflected, giving its intensity.

3. Results and discussions:

The optimized thickness taken during the result preparation is 45 nm for Au_1 film, 0.993 nm for MXene film, 3 nm for Au_2 film, and 0.34 nm for graphene film. The result obtained after

the theoretical analysis of SPR sensor design is explained in this section. Firstly, Figure 2 explains the four different scenarios of reflectance with an angle of incidence curves for the absence of MXene and graphene nanofilms ($G = 0, T = 0$) shown in Figure 2(a). Then the next cases for $G = 0, T = 1$ (i.e., in the presence of a single graphene nanofilm, no MXene film) and $G = 1, T = 0$ (i.e., with a single MXene and no graphene film) shown in Figure 2(b) and 2(c) respectively and at last with Figure 2(d) the SPR curves shown for the $G = 1, T = 1$ case(with single MXene and graphene nanofilms). All these SPR curves have been plotted considering the RI of the sensing medium as 1.33 (black line curve) and 1.34 (red line curve). With the addition of both materials films $(\mathrm{G} = \mathrm{T} = 1)$ over the traditional structure (i.e., $\mathrm{G} = \mathrm{T} = 0$), the SPR curves shift with the shift in the angle of incidence [Figure 2(d)] as compared to the traditional case. The corresponding sensitivity chart for these four cases is shown in Table 3. In Table 3, case 4 (i.e., $G = T = 1$), the sensitivity is maximum (147.2 $degree/RIU$) when compared with the other three cases (case 1,2 and 3). So the impact of adding 2D materials films over metal layers (proposed work) indicates its advantage over traditional structure (case 1) in terms of sensitivity.

Table 3. Tabulation chart for sensitivity and change in resonance angle calculation

Cases	Sensitivity (degree/RIU)	Δ θ (degree)
Case 1: $\mathbf{G = 0, T = 0}$	137.8	1.378
Case 2: $\mathbf{G = 0, T = 1}$	140.8	1.408
Case 3:$\mathbf{G = 1, T = 0}$	143.4	1.434
Case 4:$\mathbf{G = 1, T = 1}$	147.2	1.472

In Figure 3, the effect of variation of both the films (keeping one constant at a time) is shown in Figure 3. Figure 3(a) shows the impact on SPR curves by varying the graphene film (T) from 0 to 5, keeping MXene film constant. The shift in SPR curves and the shape of the SPR curve also alters (it becomes wider). The same impact can be observed in Figure 3(b). As in this case, the Mxene film kept constant, and the graphene layer varied from 0 to 5.

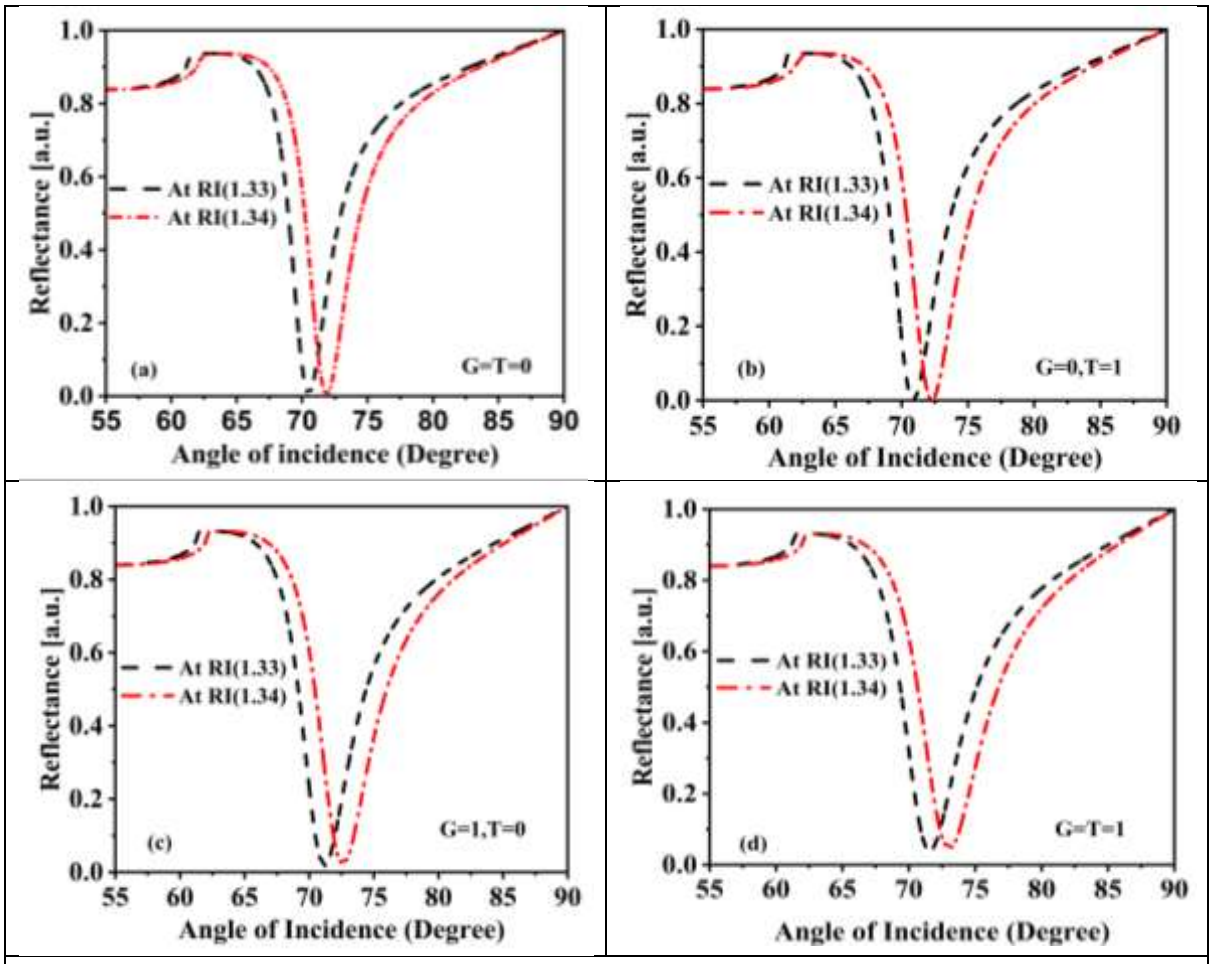

Figure 2. Reflectance as a function of angle of incidence, for (a) $G,T = 0$,0 (b) $G,T = 0,1$, (c) $G,T = 1,0$ and, (d) $G,T = 1,1$

Then, Figure 4 gives the sensitivity alteration for the four cases discussed earlier but with varying RI of 1.33 to 1.38 with a change in $RI = 0.01$. Case 1, for $G = T = 0$, the maximum and minimum sensitivity achieved is 137.8 $degree/RIU$ and 202.8 $degree/RIU$ [indicated by black dash line]. Case 2, for $G = 0$ and $T = 1$, minimum sensitivity of 140.8 $degree/RIU$ and a maximum of 202.8 $degree/RIU$ is attained [indicated by red dash line]. Case 3, for $G = 1$ and $T = 0$ the minimum and maximum sensitivity achievable is 143.4 $degree/RIU$ and 216.2 $degree/RIU$.

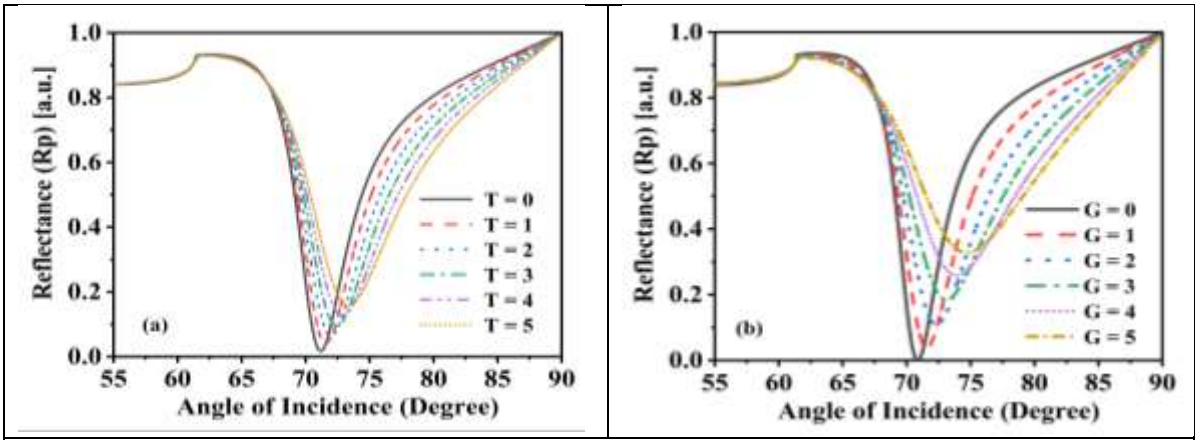

Figure 3. Reflectance as a function of angle of incidence for (a) MXene film (G) = constant and varying graphene film (T) and (b) graphene film (T) = constant and varying MXene film (G)

Finally, in the case ($G = T = 1$), the maximum and minimum sensitivity achieved is 147.2 $degree/RIU$ and 218.4 $degree/RIU$ [indicated with blue dash lines]. So, the conclusion here can be made that with the inclusion of both the nanofilms of MXene and graphene, the sensitivity increases to an extent compared to the traditional structure.

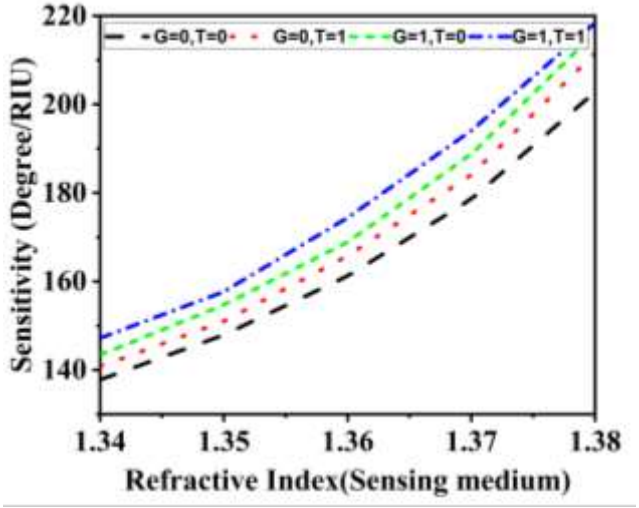

Figure 4. Sensitivity as a function of the refractive index of the sensing medium

Figure 5 shows the influence of metal layer thickness on the SPR sensor's characteristics. The graph is plotted for reflectance w.r.t the angle of incidence. For the analysis, the metal (Au_1) layer thickness is optimized. Different thicknesses of the Au1 layer were taken from 25 nm to 55 nm with a gap interval of 10, and the minimum reflectance was measured. It is to be noted that for metal (Au_1) film thickness of 45 nm, the minimum reflectance of 0.03862 has been observed with the resonance mechanism. As a result, for 45 nm thickness of the metal film sensor's performance is higher.

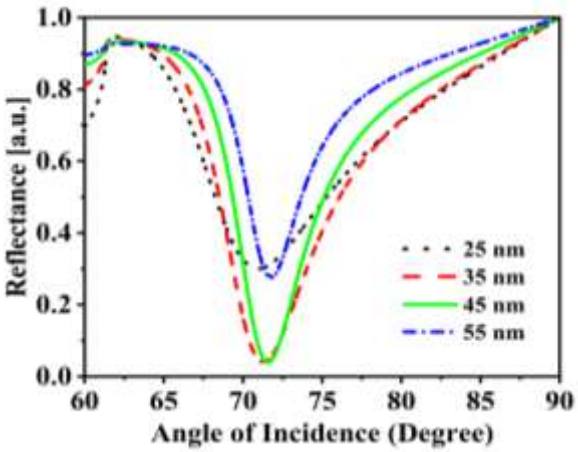

Figure 5. Reflectance v/s angle of incidence plot for different Au1 film thickness

3.1 Malaria stage detection:

For the detection of malaria disease stages, firstly, we investigated the change in reflectance characteristics with respect to incidence angle after adjusting the geometrical parameters of the proposed sensor for the four stages of the disease. The blood analyte sensor layer to detect various stages of infection with malaria is depicted in Fig. 6. The SPR curves have been shifted to a lower resonance angle. As we invaded the area, the width of these bends became wider as we infiltrated the blood with different stages of malaria (i.e., from normal stage to ring stage, ring stage to Trophozoite stage, and then finally to Schizont stage). From the normal to the schizont (highest infectious) stage of malaria, the SPR curves shift to a lower incidence angle.

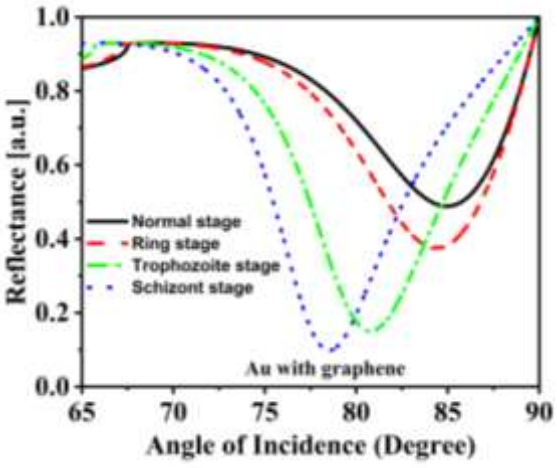

Figure 6. Impact on reflectance for the angle of incidence for various malaria stages with $d_{MXene} = 0.993$ nm, $d_{Au1} = 45$ nm and $d_{Au2} = 3$ nm

This is due to the fact that the RI shifts to lower values with different stages of malaria, from 1.402 to 1.371. Malaria detection is further being studied with the help of the plot shown in Figure 7. It gives out the resonance angle variations w.r.t. the various malaria stages (i.e., from first to last). For the first stage (normal) of malaria, the angle of resonance is on the higher side when compared with the next stages (ring to schizont).

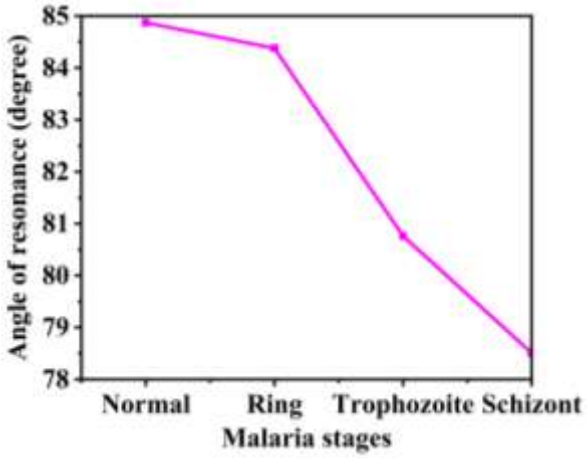

Figure 7. Impact of malaria stages on the angle of resonance

Figure 8 gives the sensitivity variation with the changes in stages of malaria for metal (Au1) film with graphene film. The maximum sensitivity value is 258.28 degree/RIU achieved for the trophozoite stage of malaria disease and a minimum (70.57 degree/RIU) for the first (ring) stage. For the schizont stage, 225.4 degree/RIU sensitivity has been achieved.

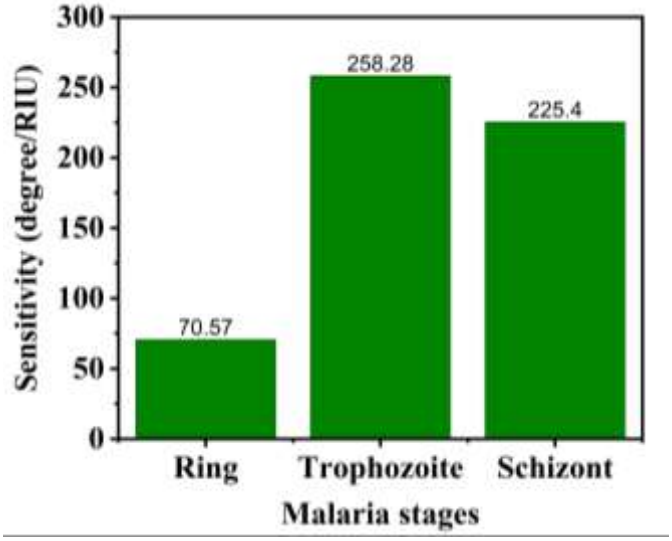

Figure 8. Sensitivity versus malaria stages curve

The upcoming table, Table 4, indicates the results obtained during the MATLAB simulation of SPR-based biosensor.

Table 4: Performance parameter's tabulation chart for different combinations of G and T

LAYERS	θ_1	θ_2	FWHM ($degree$)	DA ($degree^{-1}$)	QF (RIU^{-1})	S ($degree/RIU$)
$\mathbf{G=0, T=0}$	76.38	82.03	5.65	0.18	35.9	202.8
$\mathbf{G=0, T=1}$	76.67	83.02	6.35	0.16	33.3	211.6
$\mathbf{G=1, T=0}$	76.84	83.78	6.94	0.14	31.2	216.2
$\mathbf{G=1, T=1}$	77.25	84.52	7.27	0.14	30.0	218.4
$\mathbf{G=1, T=2}$	77.72	85.07	7.35	0.14	31.0	227.9
$\mathbf{G=1, T=3}$	78.28	85.4	7.12	0.14	31.2	222.1
$\mathbf{G=2, T=1}$	78.14	85.15	7.01	0.14	31.0	217.2
$\mathbf{G=3, T=1}$	79.55	84.64	5.09	0.20	37.4	190.5

The different combinations of layers of MXene (G) and graphene (T) were taken to calculate the performance parameters. At $\mathrm{G}=1$ and $\mathrm{T}=2$, the sensitivity value is highest ($227.9\ \mathrm{degree/RIU}$) than in other combinations of films. The minimum sensitivity for the layer combination ($G=0$ and $T=0$) (i.e., $202.8\ \mathrm{degree/RIU}$). It should also be noted that the sensitivity decreases after the $\mathrm{G}=1, \mathrm{T}=2$ combination. The values of performance parameters indicated here were all at $R.I.=1.38$ as we considered here RI variation of 0.01 for range of R.I. from 1.33 to 1.38.

3.2 Proposed and previous work analysis:

Table 5 gives the comparative analysis between the earlier studies on SPR sensors with the present study.

Table 5: Brief summarization of proposed and earlier studies

Ref.	λ	Layer designs (Prism +)	S	DA	QF	FWHM
Present study	633 nm	Au_1+MXene+Au_2+graphene ($G=1, T=2$)	227.9	0.14	31	7.35
Present study	633 nm	Au_1+MXene+Au_2+graphene (Trophozoite stage)	258.28	0.14	35.5	7.27

[28]	633 nm	Au+$PtSe_2$+graphene	200	-	-	-
[30]	633 nm	TiO_2+Ag+MoSe+graphene	194	0.2702	54.04	-
[31]	632.8 nm	TiO_2+ZnO+Au+MoS_2+GO	210.75	-	-	-
[1]	633 nm	Au+TMDC+Au+$Ti_3C_2T_x$	198	-	-	-
[49]	632 nm	Rh+Ag+Si+Graphene	220	0.098	21.56	10.204
[50]	633 nm	Ag+graphene	91.76	-	52.31	1.754

3.3 Normalized field distribution

In Figure 10, the electric field plots perpendicular to the prism interface for the proposed sensor (Au1 / MXene / Au2 / graphene). The electric field intensity increases with the inclusion of the metal layer over the prism interface, and at last, it attains maximum value at the last graphene/sensing medium interface. It is due to graphene's high biomolecular absorption rate acting as a BRE. The enhancement in an electric field is greater for the proposed sensor along with the graphene/sensing film interface. The electric field's greater interaction in the analyte region generally increases sensitivity.

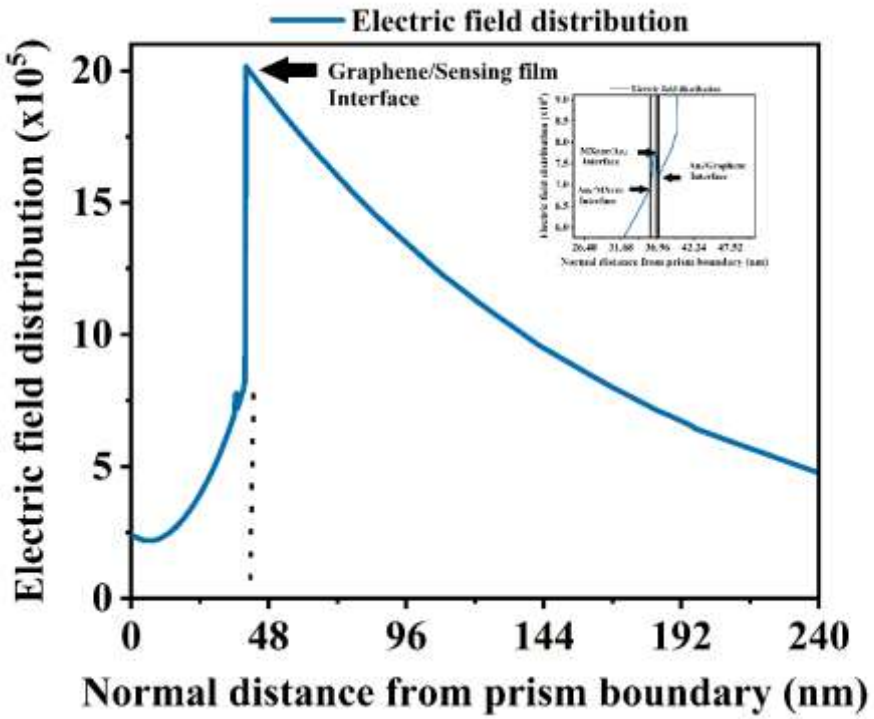

Fig. 10. Electric field distribution for proposed SPR biosensor

Conclusion:

A highly sensitive Kretschmann geometry relied on SPR biosensor has been numerically analyzed to detect all phases of malaria disease. The suggested SPR biosensor depends upon the existence of SPR that relies upon R.I. fluctuations of RBC across the life cycle of the malaria parasite. The suggested sensor's structure comprises bimetallic Au, MXene, and graphene nanofilms, which ultimately ascends the sensitivity to 227.9 degree/RIU level for the single MXene and two graphene layers compared to 202.8 degree/RIU for a traditional structure. The other performance parameters computed are DA, QF, and FWHM of 0.14 $degree^{-1}$, 31 RIU^{-1}, and 7.35 degrees. The maximum sensitivity of 258.28 degree/RIU has been calculated for the trophozoite stage with DA of 0.14 $degree^{-1}$, FWHM of 7.27 degree, and QF of 35.5 RIU^{-1}. The current research results provide a unique perspective in the research area of photonic sensors, which can be employed to diagnose malaria disease at the initial stages.

Declaration

Code Availability: Not applicable.

Funding Information: No funding available.

Conflicts of interest/Competing interests: The author declare that he has no conflict of interest.

Availability of data and material: No data available.

Authors' contributions

AU formulated the problem statement wherein giving the theoretical background and mathematical modelling for SPR biosensor. He also helped in drafting and finalizing the manuscript.

BLC provided the theoretical background to biosensing and the importance of Optical Biosensing. She also helped in finalizing the design of the proposed sensor.

AP worked towards the complete manuscript, formatting, and finalizing the manuscript. He provided the theoretical background to SPR biosensors.

Ethics approval

Not applicable. The work presented in this manuscript is mathematical modelling only for the proposed biosensor. No experiment was performed on the human body and/or living organism/ animal. So, an ethical approval from an ethical committee is not required.

Consent to participate

I am willing to participate in the work presented in this manuscript.

Consent for publication

The author has given their consent to publish this work.

References

[1] Y. Xu, Y. S. Ang, L. Wu, and L. K. Ang, "High sensitivity surface plasmon resonance sensor based on two-dimensional MXene and transition metal dichalcogenide: A theoretical study," *Nanomaterials*, vol. 9, no. 2, pp. 1–11, 2019, doi: 10.3390/nano9020165.

[2] A. Otto, "Excitation of nonradiative surface plasma waves in silver by the method of frustrated total reflection," *Zeitschrift für Phys.*, vol. 216, no. 4, pp. 398–410, 1968, doi: 10.1007/BF01391532.

[3] E. Kretschmann and H. Raether, "Radiative decay of non-radiative surface plasmons by light," *Z. Naturforsch*, vol. 23, no. a, pp. 2135–2136, 1968.

[4] A. Uniyal, B. Chauhan, A. Pal, and Y. Singh, "Surface plasmon biosensor based on Bi 2 Te 3 antimonene heterostructure for the detection of cancer cells," *Appl. Opt.*, vol. 61, no. 13, pp. 3711–3719, 2022.

[5] X. Dai, Y. Liang, Y. Zhao, S. Gan, Y. Jia, and Y. Xiang, "Sensitivity enhancement of a surface plasmon resonance with tin selenide (SnSe) allotropes," *Sensors (Switzerland)*, vol. 19, no. 173, 2019, doi: 10.3390/s19010173.

[6] B. Karki, S. Sharma, Y. Singh, and A. Pal, "Sensitivity Enhancement of Surface Plasmon Resonance Biosensor with 2-D Franckeite nanosheets," *Plasmonics*, vol. 13, pp. 1–16, 2021.

[7] X. Zhao *et al.*, "Sensitivity enhancement in surface plasmon resonance biochemical sensor based on transition metal dichalcogenides/graphene heterostructure," *Sensors (Switzerland)*, vol. 18, no. 7, 2018, doi: 10.3390/s18072056.

[8] S. N, K. B, R. KP, J. A, and P. A, "Tuning and Sensitivity Improvement of Bi-metallic

Structure-based Surface Plasmon Resonance Biosensor with 2-D ξ-Tin Selenide nanosheets," pp. 1–14, 2021, [Online]. Available: https://europepmc.org/article/ppr/ppr370506.

[9] L. K. Gifford, I. E. Sendroiu, R. M. Corn, and A. Lupták, "Attomole detection of mesophilic DNA polymerase products by nanoparticle-enhanced surface plasmon resonance imaging on glassified gold surfaces," *J. Am. Chem. Soc.*, vol. 132, no. 27, pp. 9265–9267, 2010, doi: 10.1021/ja103043p.

[10] K. M. Mayer and J. H. Hafner, "Localized surface plasmon resonance sensors," *Chem. Rev.*, vol. 111, no. 6, pp. 3828–3857, 2011, doi: 10.1021/cr100313v.

[11] M. Piliarik, L. Párová, and J. Homola, "High-throughput SPR sensor for food safety," *Biosens. Bioelectron.*, vol. 24, no. 5, pp. 1399–1404, 2009, doi: 10.1016/j.bios.2008.08.012.

[12] R. C. Jorgenson and S. S. Yee, "A fiber-optic chemical sensor based on surface plasmon resonance," *Sensors Actuators B. Chem.*, vol. 12, no. 3, pp. 213–220, 1993, doi: 10.1016/0925-4005(93)80021-3.

[13] S. K. Srivastava, R. Verma, and B. D. Gupta, "Surface plasmon resonance based fiber optic sensor for the detection of low water content in ethanol," *Sensors Actuators, B Chem.*, vol. 153, no. 1, pp. 194–198, 2011, doi: 10.1016/j.snb.2010.10.038.

[14] W. Su, G. Zheng, and X. Li, "Design of a highly sensitive surface plasmon resonance sensor using aluminum-based diffraction grating," *Opt. Commun.*, vol. 285, no. 21–22, pp. 4603–4607, 2012, doi: 10.1016/j.optcom.2012.07.026.

[15] Y. Kumar, R. Mishra, E. Panwar, J. Kaur, and R. Panwar, "Design, optimization and critical analysis of graphene based surface plasmon resonance sensor for DNA hybridization," *Opt. Quantum Electron.*, vol. 51, no. 10, 2019, doi: 10.1007/s11082-019-2057-8.

[16] N. Liu, S. Wang, Q. Cheng, B. Pang, and J. Lv, "High Sensitivity in Ni-Based SPR Sensor of Blue Phosphorene/Transition Metal Dichalcogenides Hybrid Nanostructure," *Plasmonics*, vol. 16, no. 5, pp. 1567–1576, 2021, doi: 10.1007/s11468-021-01421-w.

[17] B. Karki, A. Uniyal, B. Chauhan, and A. Pal, "Sensitivity enhancement of a graphene, zinc sulfide-based surface plasmon resonance biosensor with an Ag metal

configuration in the visible region," *J. Comput. Electron.*, no. January, 2022, doi: 10.1007/s10825-022-01854-4.

[18] A. Panda and P. D. Pukhrambam, "Modeling of High-Performance SPR Refractive Index Sensor Employing Novel 2D Materials for detection of Malaria Pathogens," *IEEE Trans. Nanobioscience*, vol. PP, no. c, pp. 1–1, 2021, doi: 10.1109/tnb.2021.3115906.

[19] F. Wu *et al.*, "Ultrasensitive and rapid detection of malaria using graphene-enhanced surface plasmon resonance," *2D Mater.*, vol. 7, no. 4, 2020, doi: 10.1088/2053-1583/aba88e.

[20] Y. Feng, Y. Liu, and J. Teng, " Design of an ultrasensitive SPR biosensor based on a graphene-MoS2 hybrid structure with a MgF2 prism ," *Appl. Opt.*, vol. 57, no. 14, p. 3639, 2018, doi: 10.1364/ao.57.003639.

[21] T. Srivastava and R. Jha, "Black Phosphorus: A New Platform for Gaseous Sensing Based on Surface Plasmon Resonance," *IEEE Photonics Technol. Lett.*, vol. 30, no. 4, pp. 319–322, 2018, doi: 10.1109/LPT.2017.2787057.

[22] X. Gan, H. Zhao, and X. Quan, "Two-dimensional MoS2: A promising building block for biosensors," *Biosens. Bioelectron.*, vol. 89, pp. 56–71, 2017, doi: 10.1016/j.bios.2016.03.042.

[23] B. Karki, A. Pal, Y. Singh, and S. Sharma, "Sensitivity enhancement of surface plasmon resonance sensor using 2D material barium titanate and black phosphorus over the bimetallic layer of Au , Ag , and Cu," *Opt. Commun.*, vol. 508, no. October 2021, p. 127616, 2022, doi: 10.1016/j.optcom.2021.127616.

[24] Y. Zhao, S. Gan, G. Zhang, and X. Dai, "High sensitivity refractive index sensor based on surface plasmon resonance with topological insulator," *Results Phys.*, vol. 14, no. June, p. 102477, 2019, doi: 10.1016/j.rinp.2019.102477.

[25] G. AK, "Graphene: status and prospects," *Science (80-.).*, vol. 324, no. 5934, pp. 1530–1534, 2009.

[26] F. Bonaccorso, Z. Sun, T. Hasan, and A. C. Ferrari, "Graphene photonics and optoelectronics," *Nat. Photonics*, vol. 4, no. 9, pp. 611–622, 2010, doi: 10.1038/nphoton.2010.186.

[27] L. Wu *et al.*, “Sensitivity Improved SPR Biosensor Based on the MoS2/Graphene-Aluminum Hybrid Structure,” *J. Light. Technol.*, vol. 35, no. 1, pp. 82–87, 2017, doi: 10.1109/JLT.2016.2624982.

[28] S. Mostufa, A. K. Paul, and K. Chakrabarti, “Detection of hemoglobin in blood and urine glucose level samples using a graphene-coated SPR based biosensor,” *OSA Contin.*, vol. 4, no. 8, p. 2164, 2021, doi: 10.1364/osac.433633.

[29] K. Dong *et al.*, “High sensitivity SPR sensor for liquid phase sample with Ag/PbS/Graphene hybrid nanostructure,” *Guangdian Gongcheng/Opto-Electronic Eng.*, vol. 44, no. 2, pp. 198–201, 2017, doi: 10.3969/j.issn.1003-501X.2017.02.008.

[30] M. Moznuzzaman, I. Khan, and M. R. Islam, “Nano-layered surface plasmon resonance-based highly sensitive biosensor for virus detection: A theoretical approach to detect SARS-CoV-2,” *AIP Adv.*, vol. 11, no. 6, pp. 1–10, 2021, doi: 10.1063/5.0046574.

[31] S. Guo, X. Wu, Z. Li, and K. Tong, “High-Sensitivity Biosensor-Based Enhanced SPR by ZnO/MoS2Nanowires Array Layer with Graphene Oxide Nanosheet,” *Int. J. Opt.*, vol. 2020, 2020, doi: 10.1155/2020/7342737.

[32] B. Anasori, M. R. Lukatskaya, and Y. Gogotsi, “2D metal carbides and nitrides (MXenes) for energy storage,” *Nat. Rev. Mater.*, vol. 2, no. 2, 2017, doi: 10.1038/natrevmats.2016.98.

[33] M. R. Lukatskaya *et al.*, “Ultra-high-rate pseudocapacitive energy storage in two-dimensional transition metal carbides,” *Nat. Energy*, vol. 6, no. July, pp. 1–6, 2017, doi: 10.1038/nenergy.2017.105.

[34] M. Naguib, V. N. Mochalin, M. W. Barsoum, and Y. Gogotsi, “25th anniversary article: MXenes: A new family of two-dimensional materials,” *Adv. Mater.*, vol. 26, no. 7, pp. 992–1005, 2014, doi: 10.1002/adma.201304138.

[35] A. Lipatov, M. Alhabeb, M. R. Lukatskaya, A. Boson, Y. Gogotsi, and A. Sinitskii, “Effect of Synthesis on Quality, Electronic Properties and Environmental Stability of Individual Monolayer Ti3C2 MXene Flakes,” *Adv. Electron. Mater.*, vol. 2, no. 12, 2016, doi: 10.1002/aelm.201600255.

[36] Ankita, B. Suthar, and A. Bhargava, “Biosensor Application of One-Dimensional

Photonic Crystal for Malaria Diagnosis," *Plasmonics*, vol. 16, no. 1, pp. 59–63, 2021, doi: 10.1007/s11468-020-01259-8.

[37] N. Tangpukdee, C. Duangdee, P. Wilairatana, and S. Krudsood, "Malaria diagnosis: A brief review," *Korean J. Parasitol.*, vol. 47, no. 2, pp. 93–102, 2009, doi: 10.3347/kjp.2009.47.2.93.

[38] S. Bendib and B. C, "Photonic Crystals for Malaria Detection," *J. Biosens. Bioelectron.*, vol. 09, no. 03, 2018, doi: 10.4172/2155-6210.1000257.

[39] M. A. Agnero *et al.*, "Malaria-infected red blood cell analysis through optical and biochemical parameters using the transport of intensity equation and the microscope's optical properties," *Sensors (Switzerland)*, vol. 19, no. 14, 2019, doi: 10.3390/s19143045.

[40] P. S. Pandey, Y. Singh, and S. K. Raghuwanshi, "Theoretical analysis of the LRSPR sensor with Enhance FOM for Low Refractive Index Detection using MXene and Fluorinated Graphene," *IEEE Sens. J.*, vol. 21, no. 21, pp. 23979–23986, 2021, doi: 10.1109/JSEN.2021.3112530.

[41] P. Bhatia and B. D. Gupta, "Refractive Index Sensor : Sensitivity Enhancement," *Appl. Opt.*, vol. 50, no. 14, pp. 2032–1036, 2011.

[42] Y. Singh and S. K. Raghuwanshi, "Titanium dioxide (TiO2) coated optical fiber-based SPR sensor in near-infrared region with bimetallic structure for enhanced sensitivity," *Optik (Stuttg).*, vol. 226, no. P1, p. 165842, 2021, doi: 10.1016/j.ijleo.2020.165842.

[43] T. B. A. Akib *et al.*, "Design and numerical analysis of a graphene-coated spr biosensor for rapid detection of the novel coronavirus," *Sensors*, vol. 21, no. 10, pp. 1–21, 2021, doi: 10.3390/s21103491.

[44] A. Pal and A. Jha, "A theoretical analysis on sensitivity improvement of an SPR refractive index sensor with graphene and barium titanate nanosheets," *Optik (Stuttg).*, vol. 231, no. January, 2021, doi: 10.1016/j.ijleo.2021.166378.

[45] A. Shalabney and I. Abdulhalim, "Electromagnetic fields distribution in multilayer thin film structures and the origin of sensitivity enhancement in surface plasmon resonance sensors," *Sensors Actuators, A Phys.*, vol. 159, no. 1, pp. 24–32, 2010, doi: 10.1016/j.sna.2010.02.005.

[46] S. Y. Chuang, H. L. Chen, S. S. Kuo, Y. H. Lai, and C. C. Lee, “Using direct nanoimprinting to study extraordinary transmission in textured metal films,” *Opt. Express*, vol. 16, no. 4, p. 2415, 2008, doi: 10.1364/oe.16.002415.

[47] B. Dey, M. S. Islam, and J. Park, “Numerical design of high-performance WS2/metal/WS2/graphene heterostructure based surface plasmon resonance refractive index sensor,” *Results Phys.*, vol. 23, no. November 2020, p. 104021, 2021, doi: 10.1016/j.rinp.2021.104021.

[48] P. Chen, N. Li, X. Chen, W. J. Ong, and X. Zhao, “The rising star of 2D black phosphorus beyond graphene: Synthesis, properties and electronic applications,” *2D Mater.*, vol. 5, no. 1, 2018, doi: 10.1088/2053-1583/aa8d37.

[49] A. K. Mishra and S. K. Mishra, “Gas sensing in Kretschmann configuration utilizing bi-metallic layer of Rhodium-Silver in visible region,” *Sensors Actuators B. Chem.*, vol. 237, pp. 969–973, 2016, doi: 10.1016/j.snb.2016.07.041.

[50] P. K. Maharana, P. Padhy, and R. Jha, “On the Field Enhancement and Performance of an Ultra-Stable SPR Biosensor Based on Graphene,” *IEEE PHOTONICS Technol. Lett.*, vol. 25, no. 22, pp. 2156–2159, 2013.